

## Seismic response analysis of an unanchored vertical vaulted-type tank

Rulin Zhang<sup>\*1</sup>, Xudong Cheng<sup>1a</sup>, Youhai Guan<sup>1b</sup> and Alexander A. Tarasenko<sup>2c</sup>

<sup>1</sup>College of Pipeline and Civil Engineering, China University of Petroleum (East China),  
Qingdao Shandong 266580, People's Republic of China

<sup>2</sup>Industrial University of Tyumen, 38 Volodarskogo st., Tyumen, 625000, Russia

(Received June 23, 2016, Revised July 7, 2017, Accepted July 14, 2017)

**Abstract.** Oil storage tanks are vital life-line structures, suffered significant damages during past earthquakes. In this study, a numerical model for an unanchored vertical vaulted-type tank was established by ANSYS software, including the tank-liquid coupling, nonlinear uplift and slip effect between the tank bottom and foundation. Four actual earthquakes recorded at different soil sites were selected as input to study the dynamic characteristics of the tank by nonlinear time-history dynamic analysis, including the elephant-foot buckling, the liquid sloshing, the uplift and slip at the bottom. The results demonstrate that, obvious elephant-foot deformation and buckling failure occurred near the bottom of the tank wall under the seismic input of Class-I and Class-IV sites. The local buckling failure appeared at the location close to the elephant-foot because the axial compressive stress exceeded the allowable critical stress. Under the seismic input of Class-IV site, significant nonlinear uplift and slip occurred at the tank bottom. Large amplitude vertical sloshing with a long period occurred on the free surface of the liquid under the seismic wave record at Class-III site. The seismic properties of the storage tank were affected by site class and should be considered in the seismic design of large tanks. Effective measures should be taken to reduce the seismic response of storage tanks, and ensure the safety of tanks.

**Keywords:** storage tank; seismic response; tank-liquid coupling; site class; uplift; liquid sloshing

### 1. Introduction

Normally, cylindrical steel storage tanks are very important components, principally in water supply, nuclear plants, refineries and petrochemical facilities. However, once these tanks suffer earthquake damage, significant leakage of flammable liquids, fire, explosion, poisoning and other devastating secondary disasters may occur. Past earthquakes made numerous damages and destructions to this type of structures (Cooper and Wachholz 1999). The importance goes beyond its economic cost because the effects of a failure are not limited to the risk of human lives and equipment in the proximity, but also can lead to serious consequences on the environment (Curadelli 2013). Considering the economic costs and ease of construction, real tanks often use an unanchored type that is placed directly on the free foundation. For unanchored tanks, it is difficult to offset overturning forces caused by earthquakes only relying on its gravity. The outer edge of the base plate may be lifted and separated from the foundation, and then uplift occurs and causes failure of the tank. It is of great importance to study the nonlinear uplift effect of the tank bottom.

Currently, the seismic study of tanks mostly uses the

simplified Mass Spring Model (MSM) based on the theoretical model of Haroun-Housner (Haroun 1983). Goudarzi and Sabbagh-Yazdi (2009) studied the calculation accuracy of a simplified MSM in the seismic response of tanks. The results showed the simplified MSM did not always provide accurate results for conventionally constructed tanks. Based on the mechanical model with fluid masses and convective spring stiffness given by Newmark and Rosenblueth (1971), Seleemah *et al.* (2011) investigated the seismic response of elevated broad and slender liquid storage tanks isolated by elastomeric or sliding bearings, and studied the accuracy of predictions of SAP2000 vs. 3DBASIS-ME programs. However, these simplified models are difficult to obtain the stress and strain distribution of the tank wall and cannot reflect the buckling failure on the tank wall and other issues.

Actually, the seismic problems of tanks belong to three-dimensional spatial problems, and the dynamic performance of tanks is very complicated. It is difficult to use the simplified method for unanchored tanks due to the nonlinear contact effect at the tank bottom. Bayraktar *et al.* (2010) studied the issue of the tank uplift and showed that the displacement and stress response became more obvious after uplift. Hosseinzadeh *et al.* (2013) compared the seismic assessment of existing steel oil storage tanks by API650-2008 provisions with finite element method (FEM) analyses. Moeindarbari *et al.* (2014) investigated multiple level performance of seismically isolated elevated storage tank isolated with multi-phase friction pendulum bearing, and used different friction coefficients, pendulum radii and

\*Corresponding author, Ph.D. Lecturer

E-mail: [zhangrulin@upc.edu.cn](mailto:zhangrulin@upc.edu.cn)

<sup>a</sup>Professor

slider displacement capacities to study seismic performance of isolated elevated storage tank with multi-phase friction pendulum. Li *et al.* (2015) adopted ABAQUS to trace the dynamic response of reinforced concrete storage tank, and investigated the dynamic characteristics and failure modes of the tank by considering the rebar's effect. Ormeño *et al.* (2015) used the procedures of three design specifications and studied the seismic response of tanks subjected to scaled ground motions, in terms of base shear, overturning moment and wall stresses. Park *et al.* (2016) presented dynamic test results of a cylindrical liquid storage tank under horizontal earthquake excitation to investigate its dynamic behavior characteristics including beam-type and oval-type vibration. The previous literatures show that few studies focused on the effect of site class on the seismic performance of unanchored tanks. However, the interaction between site class and seismic response parameters is still unclear, which include the effect on the elephant-foot buckling, the base shear, the liquid sloshing, the uplift and slip at the bottom. Therefore, it is necessary to study seismic performance of unanchored tanks to prevent structural failures when earthquakes occur.

The purpose of this study is to investigate the seismic performance under earthquakes recorded at different types of soil site. A numerical model of an unanchored tank is established, in which the liquid sloshing, the liquid-tank coupling effect, and the contact effect between the tank bottom and foundation are all considered. Through studying the seismic response of tanks with the input of four seismic waves, a comprehensive analysis of the influence of site class on the seismic performance is carried out. The study results are expected to provide reference for the seismic design of tanks, which helps to protect people's lives and ensure the safety of property.

## 2. Modeling of fluid-tank-foundation system based on Lagrangian approach

Under the action of strong earthquakes, fierce collision may occur between the liquid and tank wall. Due to the constraint role of the tank wall, the liquid in the tank will be shaking in a substantially vertical manner. It considers the coupling relationship between the liquid and the tank wall in this study. Problems of fluid-structure interaction can be investigated by using different techniques such as added mass, Lagrangian, Eulerian, and Lagrangian-Eulerian approaches in the FEM or by the analytical methods. In this study, displacement based Lagrangian approach is selected to model the fluid-tank interaction.

The equation of motion controlling the fluid-tank-foundation system can be written as

$$\begin{aligned} & ([\mathbf{M}_{st}] + [\mathbf{M}_f])\{\ddot{u}(t)\} + ([\mathbf{C}_{st}] + [\mathbf{C}_f])\{\dot{u}(t)\} \\ & + ([\mathbf{K}_{st}] + [\mathbf{K}_f] + [\mathbf{K}_s])\{u(t)\} = -([\mathbf{M}_{st}] + [\mathbf{M}_f])\{a_g(t)\} \end{aligned} \quad (1)$$

where,  $\mathbf{M}$ ,  $\mathbf{K}$  and  $\mathbf{C}$  are the mass, stiffness and damping matrix subscripts st, f, and s, indicate foundation-structure, fluid, and fluid surface of the fluid-tank-foundation system, respectively.  $\{a_g\}$  is the input seismic acceleration. More

details can be found in the study (Livaoglu and Dogangun 2007).

When modelling the fluid-structure interaction, the radial degrees-of-freedom are coupled between the liquid elements and the tank wall elements at the same location, coupling the vertical degrees-of-freedom at the same location of the tank bottom. In this way, along the tank wall, the shell and the fluid can keep the displacement coordination in the tangential direction, with no mutual penetration in the radial direction. In this paper, tank contents were modeled by Fluid-80 element with ability to consider fluid-structure interaction and applied acceleration. The Fluid-80 element is particularly well suited for calculating hydrostatic pressures and fluid-solid interactions.

## 3. Description of the vertical vaulted-type tank

### 3.1 Design parameters and numerical simulation method

A vertical steel vaulted-type tank is considered in the seismic analysis. The calculation parameters are listed in Table 1. The design of the tank wall uses a variable cross section, and the thickness of the tank wall is divided into 4 segments, which are 12 mm, 10 mm, 8 mm and 6 mm from the bottom. The steel reinforcing ring uses angle steel 100×63×8. The steel tank uses Q235, The elastic modulus is 206 GPa and the yield stress is 235 MPa. The stress and strain relation of the steel material is chosen as an ideal elastoplastic model. The material parameters of the tank and selected elements are listed in Table 2.

The seismic analysis of tank is carried based on ANSYS software (ANSYS software 2007), and the FEM model of the tank is shown in Fig. 1.

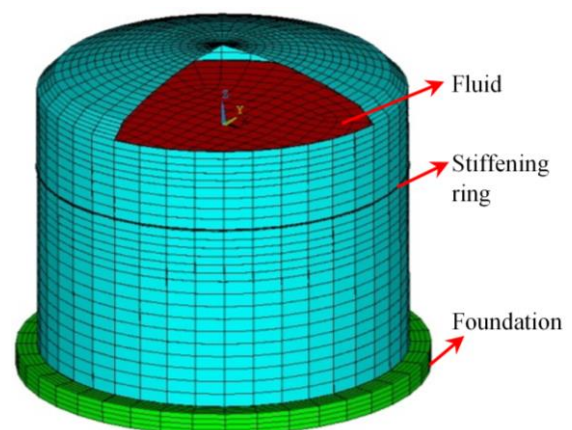


Fig. 1 The FEM model of the storage tank

Table 1 The geometric parameters of the tank

Location	Inner Diameter (m)	Total Height (m)	Tank Wall Height (m)	Vault Height (m)	Liquid Height (m)	Thickness of Vault (mm)
Value	18.9	14.55	12.3	2.25	10.5	6

Table 2 Material parameters and selected elements for the FEM model of tank

Location	Density (kg/m <sup>3</sup> )	Elastic Modulus (GPa)	Poisson's Ratio	Element
Tank wall	7800	206	0.30	Shell-181
Liquid	1000	2.04	—	Fluid-80
Stiffening ring	7800	206	0.30	Beam-188
Foundation	2400	30	0.26	Solid-45
Tank roof	7800	206	0.30	Shell-181

Table 3 Records of earthquakes and ground motion parameters

Site Class	Earthquake Name	Recording Stations	PGA(g)
Class-I	Northridge 1994/01/17	Lake Hughes #9	0.217
Class-II	Parkfield 1966/06/28	Temblor pre-1969	0.357
Class-III	Borrego Mtn 1968/04/09	El Centro Array #9	0.133
Class-IV	Kobe 1995/01/16	Kakogawa	0.251

When modeling the liquid-tank coupling, at the tank bottom, the fluid is allowed to slide along the horizontal direction, and in the meantime, the fluid is not allowed to penetrate in the vertical direction. In a strong earthquake, nonlinear uplift may appear between the foundation and tank bottom. In this study, a further assumption is incorporated into the model for unanchored tanks, i.e., the Gap element (ANSYS Inc 2012) is adopted to model the uplift. Face-to-face contact between the tank bottom and the foundation platform is adopted, and the contact element and the target element that are matched with the shell element and the solid element are selected. The target element is set at the tank bottom, and the contact element is set on the surface of the foundation. When calculating, the friction coefficient is 0.2. The ground motion is input at the foundation bottom, which is fixed by three directions of X, Y and Z.

### 3.2 Seismic waves recorded at different types of sites

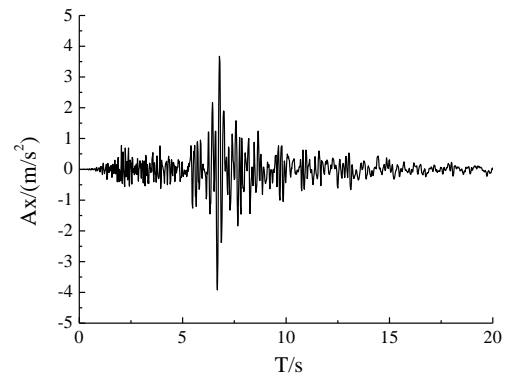
The seismic response of the tank structure has a relationship not only with the peak acceleration of the ground motion but also with the duration of the earthquake, the characteristics of the site soil, and the predominant period of the seismic wave. According to the shear wave velocity of the ground soil that is more than 750 m/s, 360-750 m/s, 180-360 m/s and less than 180 m/s, the earthquake records are divided into four groups by the United States Geological Survey (Ma *et al.* 2008). Four earthquake records at different types of sites are selected from the earthquake database of the University of California, which are listed in Table 3.

To study the seismic response characteristics of the tank liquid coupling system including the dynamic response and

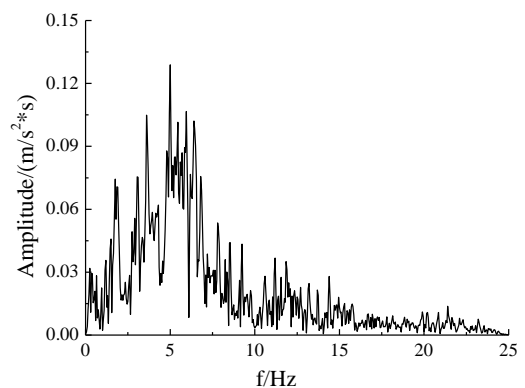
strength destruction under different site conditions, the PGA of each seismic wave is uniformly adjusted to 9 degrees of seismic intensity, namely, PGA unified is adjusted to 0.4 g, according to the latest Chinese national standard "Code for design of vertical cylindrical welded steel oil tanks" (GB50341-2014 2014). Moreover, the original recorded time of the seismic waves is very long. To save computing time, the duration of four seismic waves is appropriately cut off at 20 s, 10 s, 40 s and 20 s. Here, only the given acceleration time-history curves of earthquakes recorded at Class- I and Class-III sites and their corresponding Fourier spectra are shown in Figs. 2-3.

The seismic wave recorded at the Class- I site belongs to the pulse type of seismic wave, and the energy is concentrated in the high frequency portion ( $f = 5$  Hz ). However, for the Class-III site, the acceleration attenuation becomes slow after the peak value of the seismic waves. Due to the effect of the soft soil, its energy is concentrated in the low frequency portion ( $f = 0.6$  Hz ), with very few high frequency components.

In this paper, under the input of the four seismic waves in Table 3, nonlinear time-history analyses of the studied tanks were conducted using Newmark- $\beta$  method (Newmark 1959). Since the time-history analysis was time-consuming and, in some cases, even impossible due to the large number of elements, the reduced method was utilized to overcome this problem. In addition, postulated damping in time-history analyses was based on Rayleigh damping assumptions (Liu and Gorman 1995).

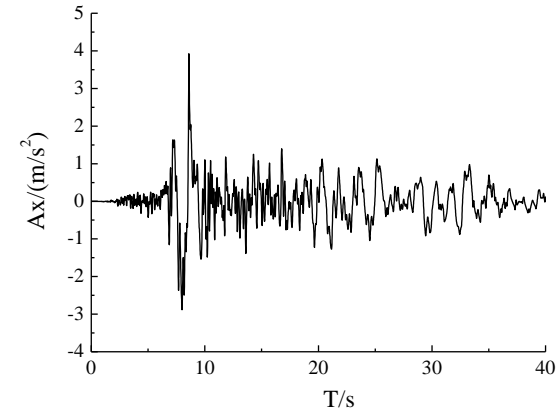


(a) Seismic wave acceleration

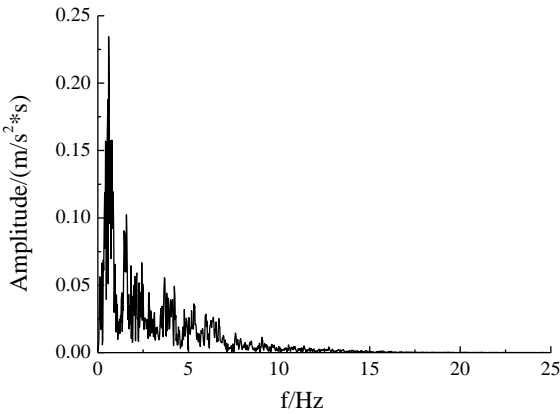


(b) Fourier spectrum of the seismic wave

Fig. 2 The acceleration and Fourier spectrum of a seismic wave at the Class-I site



(a) Seismic wave acceleration



(b) Fourier spectrum of the seismic wave

Fig. 3 The acceleration and Fourier spectrum of a seismic wave at the Class-III site

#### 4. Modal analysis of the tank liquid coupling system

The modal analysis can verify the rationality of the FEM model. Assuming that the tank is rigid, that the liquid is ideal and incompressible, and that the ground movement is a horizontal translation movement, there is no rotational component. The basic convection mode  $f_w$  of liquid sloshing can be obtained based on the second linear solution of the Laplace equation by (Veleros and Yang 1977). The vibration of the liquid-solid coupling system is described by a vibrational principle, and the fundamental mode  $f_c$  of the liquid tank coupling vibration can be solved (Udwadia and Tabaie 1981). The theoretical formula of  $f_w$  and  $f_c$  are shown in Eqs. (2)-(3), respectively

$$f_w = \frac{1}{2\pi} \sqrt{\lambda_1 \frac{g}{R} \tanh\left(\lambda_1 \frac{H}{R}\right)} \quad (2)$$

$$f_c = \frac{1}{2\pi} \sqrt{\frac{E t_s}{\rho_l R^3} \left(\alpha_1 \frac{R}{H}\right) \frac{I_1\left(\alpha_1 \frac{R}{H}\right)}{I_0\left(\alpha_1 \frac{R}{H}\right)}} \quad (3)$$

where  $\lambda_1$  is the root of the derivative of the first-order Bessel function (1.841),  $R$  is the radius of the tank,  $H$  is the height of the liquid,  $g$  is the gravitational acceleration,  $I_1$  and  $I_0$  are the first-order and the 0-order, respectively, of the

Table 4 Coefficients of the sloshing period and coefficients of the coupling vibration period

$D/H_w$	0.6	1.0	1.5	2.0	2.5	3.0
$K_s$	1.047	1.047	1.054	1.074	1.105	1.141
$K_c(*10^{-3})$	0.514	0.44	0.425	0.435	0.461	0.502
$D/H_w$	3.5	4.0	4.5	5.0	5.5	6.0
$K_s$	1.184	1.230	1.277	1.324	1.371	1.418
$K_c(*10^{-3})$	0.537	0.58	0.62	0.681	0.736	0.791

Table 5 Comparison of the natural frequency results of the storage tank model

Natural Frequency	Numerical Results ( $H_z$ )	Theoretical Calculation Results		Standardized Recommendations	
		Results ( $H_z$ )	Error (%)	Results ( $H_z$ )	Error (%)
$f_w$	0.228	0.216	5.56	0.216	5.56
$f_c$	7.046	7.084	0.54	7.188	1.98

first category of correction of the Bessel function, and  $\alpha_1$  is equal to  $0.5\pi$ .

According to the ‘‘Code for design of vertical cylindrical welded steel oil tanks’’, the calculation formula of the fundamental sloshing period and the liquid-tank coupling vibration period are recommended, and these parameters are calculated in Eqs. (4)-(5)

$$T_w = K_s \sqrt{D} \quad (4)$$

$$T_c = K_c H_w \sqrt{\frac{R}{\delta_{1/3}}} \quad (5)$$

where  $R$  is the inner radius of the tank,  $\delta_{1/3}$  is the calculation thickness at the 1/3 height of the tank from bottom plate,  $D$  is the inner diameter of the tank,  $H_w$  is the design level height of the liquid,  $K_c$  is the coefficient of the coupling vibration period,  $K_s$  is the coefficient of the sloshing period, and  $K_c$  and  $K_s$  can be obtained according to  $D/H_w$  by linear interpolation in Table 4.

The comparison of modal results among the numerical calculation, the theoretical calculation and the national standard is listed in Table 5. The numerical results are very close to the theoretical values and the national standard values, and the maximum error is only 5.56%. Therefore, the reasonableness is verified for using the simulation method for the tank liquid system.

#### 5. Results of the seismic response and discussion

##### 5.1 Horizontal displacement of the tank wall

Slip may occur between the tank bottom and the foundation. In this paper, the relative displacement of the tank is obtained from the displacement of the location of the tank wall minus the corresponding displacement at the bottom, and the following displacement in this paper refers to the relative displacement. The selected symmetric points

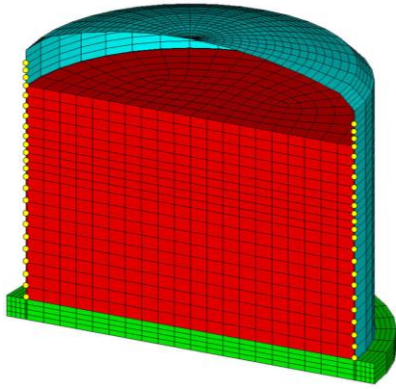


Fig. 4 The selected points on the tank wall

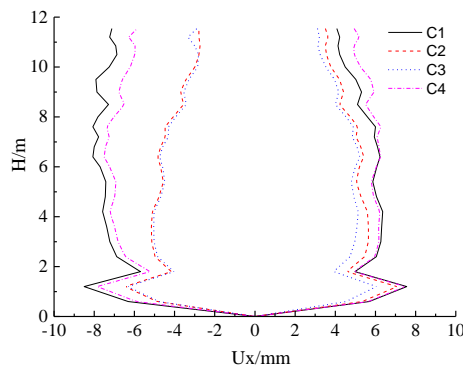


Fig. 5 The horizontal displacement distribution along the height of the tank wall

on the tank wall are shown in Fig. 4.

The time when the maximum displacement occurs at each location point is not the same under different site conditions. This study focuses on the maximum relative displacement of the tank wall. Fig. 5 displays the relative displacement distribution along the tank wall under different site conditions, as well as the time corresponding to the maximum horizontal displacement near the bottom. The symbols C1, C2, C3, and C4 represent the results under the input of earthquakes recorded at the sites of Class-I, Class-II, Class-III, and Class-IV, respectively.

According to Fig. 5, the displacement of the left tank wall is slightly larger than the displacement of the right tank wall. The difference in the displacements is smaller on the right tank wall. The maximum deformation is 8.5 mm, which occurs on the left tank wall at the Class-I site.

Overall, the displacement near the tank bottom is relatively small due to the constrained role of the bottom plate to the tank wall. However, the displacement increases rapidly as the location moves away from the tank bottom. The elephant-foot deformation occurs at 1.2 m from the tank bottom. There is a sudden reduction of the horizontal deformation at 1.8 m along the elephant-foot upward from the tank bottom, followed by a sharp increase, indicating that there is a mutation deformation. Under the action of seismic waves, there is a large axial compressive stress, which results in the local elephant-foot buckling of the tank wall. With the distance closer to the tank top, because of the ring constraints of the roof structure, the horizontal

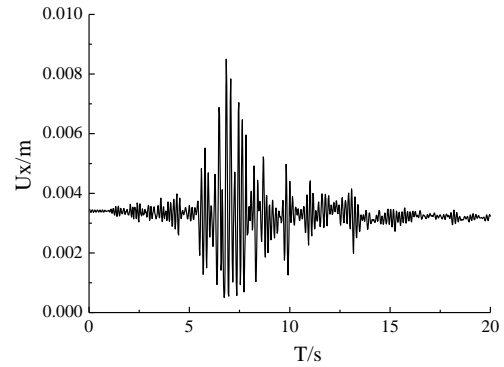


Fig. 6 The horizontal displacement at the biggest elephant-foot position

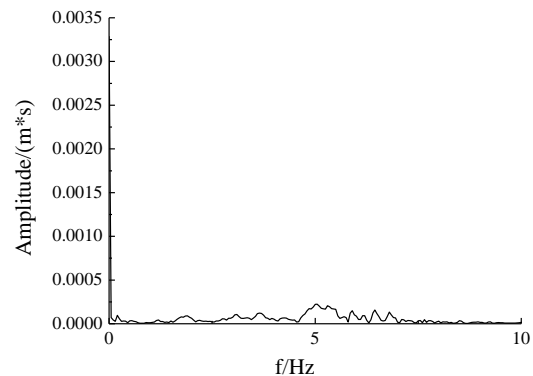


Fig. 7 Fourier spectrum of the horizontal displacement at the biggest elephant-foot position

displacement near the tank roof becomes smaller, and this is very obvious at the Class-III and Class-IV sites. After the effect of the reinforcing ring, the deformation decreases at 8.5 m from the tank bottom.

The relative horizontal displacement curve at the biggest elephant-foot position and its Fourier spectrum curve are displayed in Figs. 6-7.

Spectral analysis is carried out for the deformation at the elephant-foot. The slip occurs between the tank bottom and the foundation, which causes an overall rigid movement of the tank, and in the Fourier spectral curve, it is large amplitude at the frequency of 0. The Fourier spectrum curve also shows that another peak value occurs in the range of 5-6 Hz. According to the previous analysis, the seismic predominant frequency at the Class-I site is 5.0 Hz, and it is closer to 7.04 Hz than other three cases, which is the coupling vibration frequency of the liquid-solid coupling. Because the liquid-solid coupling vibration modes have a great impact on the horizontal deformation of the tank, the seismic wave at the Class-I site can stimulate the basic model of the liquid-solid coupling vibration and cause a larger deformation on the tank wall.

## 5.2 Stress analysis of the tank

The distribution of radial stress, hoop stress, the axial compressive stress and equivalent stress along the height of the tank wall are studied, which are displayed in Figs. 8(a)-(d).

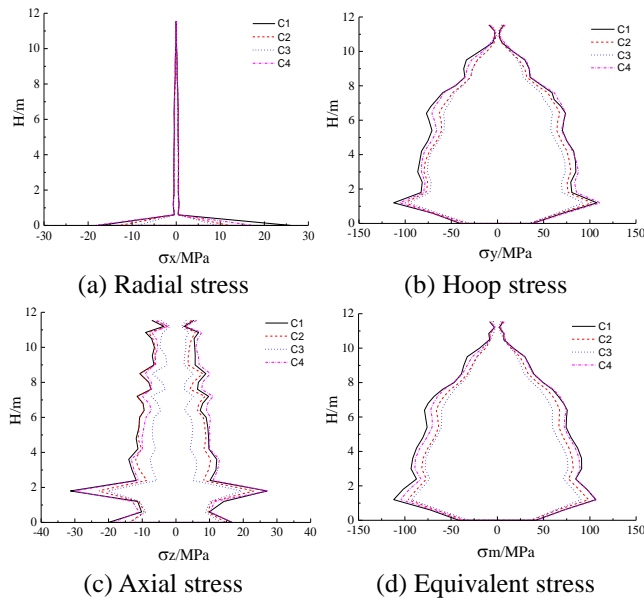


Fig. 8 Seismic stress distribution along the height of the tank wall

### 5.2.1 Radial stress

It can be seen from Fig. 8(a), due to the confined effect of the tank bottom to the tank wall structure, radial stress reaches its peak value at the connecting area of the tank wall bottom and the foundation, and the maximum radial stress reaches 26 MPa. With the increasing height from the tank bottom, radial stress decreases sharply, and the value becomes very small, much smaller than the other stresses.

### 5.2.2 Hoop stress

Fig. 8(b) shows that the hoop stress distribution along the height of the tank wall is different from radial stress. There is a greater circumferential tensile stress on the tank wall due to the obvious hydrodynamic pressure effect near the tank bottom. Hoop stress increases rapidly from the tank bottom, and at 1.2 m away from the tank bottom, and reaches the peak value (the elephant-foot position). For the four cases, the maximum hoop stresses are 112.36 MPa, 102.30 MPa, 96.25 MPa and 111.40 MPa. Obviously, this stress is much larger than the others, with hoop stress occurring at the peak maximum of the Class-I site.

As the height increases, the hydrodynamic pressure decreases, and hoop stresses have been reduced, becoming 0 near the tank top, which shows a triangular distribution. In addition, hoop stress at 3 m and 6 m becomes small due to the verity of the tank wall thickness. The decreasing trend of the stress is reduced at the 8.5 m height due to the confinement of the strengthening ring.

### 5.2.3 Axial stress

Fig. 8(c) presents that the axial stress distribution along the tank wall is different from the trend of hoop stress, and the axial stress reaches its peak at 1.8 m from the tank bottom. The maximum axial compressive stresses are 31.29 MPa, 23.24 MPa, 20.21 MPa, and 30.26 MPa, far less than hoop stress. From the point of view of the distribution, there is a significant change in peak axial stress, and axial stress

decreases rapidly after crossing the step. With the height increases, axial stress decreases rapidly and gradually stabilizes. Near the tank wall bottom, axial stress reaches its maximum and is approximately 5 times the axial stress at the top of the tank wall. The positions of peak axial stress and hoop stress (also the position of the elephant-foot) do not coincide, and the position of the peak axial stress is slightly upward, consistent with the position of the axial buckling at the bottom of the tank wall. The study also shows that the deformation of the elephant-foot near the tank bottom is the result of the combined action of the axial compressive stress and the hoop tensile stress.

### 5.2.4 Equivalent stress

According to Fig. 8(d), due to the outward pressure of the liquid and out-plane buckling of the tank wall, the tensile stress will cause its ring to make up for the part of axial compressive stress. Therefore, hoop stress is much higher than axial stress. The equivalent stress distribution is consistent with hoop stress, and maximum stress occurs near the tank bottom, that is, the occurrence of the elephant-foot deformation. The maximum stresses of the tank wall are 111.99 MPa, 98.56 MPa, 92.55 MPa, and 107.32 MPa.

### 5.2.5 Checking the calculation of stress

Based on the previous analysis, all the hoop stress, equivalent stress is less than the tank's yield stress 235MPa. Therefore, maximum stress at the elephant-foot does not yield, and no material yield damage occurs in the end.

In accordance with the code (GB50341-2014 2014), the stress of the tank wall should be less than the allowable critical axial compressive stress, and the allowable critical stress of the tank wall under earthquakes should be calculated as Eq. (6)

$$[\sigma_{cr}] = 0.22E \frac{t}{D} \quad (6)$$

where  $[\sigma_{cr}]$  is the allowable critical stress for the tank wall, MPa;  $E$  is the elastic modulus of the bottom material at the design temperature, MPa;  $t$  is the effective thickness of bottom shell, m; and  $D$  is the inner diameter of the tank, m.

The calculated allowable critical stress  $[\sigma_{cr}]$  is 28.77 MPa according to the Eq. (6). The calculated results of axial stress and yield stress of the tank wall under the four types of site conditions are listed in Table 6.

The maximum axial stresses at Class-I and Class-IV sites are 31.29 MPa and 30.26 MPa, respectively, beyond the allowable stress. For these two cases, the local buckling instability failure occurs on the tank wall. Although the

Table 6 The results of axial stress and allowable stress

Site Class	Axial Stress (MPa)	Specification Critical Stress (MPa)	Buckling or Not
Class-I	31.29	28.77	Yes
Class-II	23.24	28.77	Not
Class-III	20.21	28.77	Not
Class-IV	30.26	28.77	Yes

axial compressive stress at the Class-II site does not exceed the allowable stress, it is already in a high state of stress and are close to a risk.

**5.3 Uplift and slippage between tank bottom and foundation**

Under strong earthquake, if the overturning moment exceeds the resistance moment of the tank, the edge of the tank bottom will be separate from the foundation. For the unanchored tank, the uplift will change the distribution of the original stress field, and the possibility of failure may increase, causing leakage of fluid.

Due to seismic excitation and the effect of hydrodynamic pressure, lateral slip occurs between the tank bottom and the foundation. With sliding performance between the tank bottom and the foundation, the earthquake reduces the seismic response of the tank plate. The left and right end positions at the tank bottom are selected to analyze the uplift deformation. The time-history curve of maximum uplift and slip at the tank bottom are displayed in Fig. 9. According to Fig. 9(a), the abundant uplift response occurs at the tank bottom in four seismic waves. Fig. 9(b) shows that in the stage of the pre-earthquake, the tank has experienced sliding deformation many times and that the slip gradually stabilizes late in the late stage. The slip

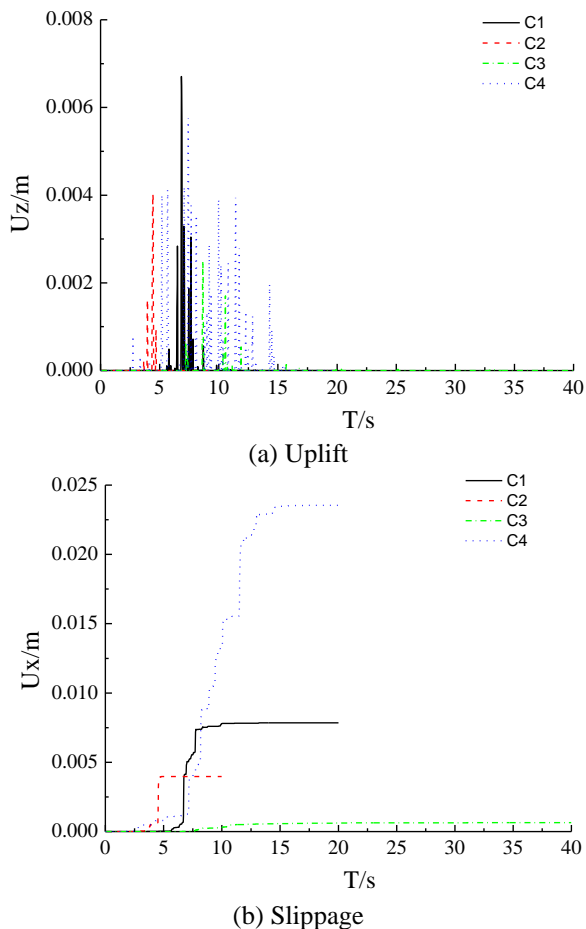
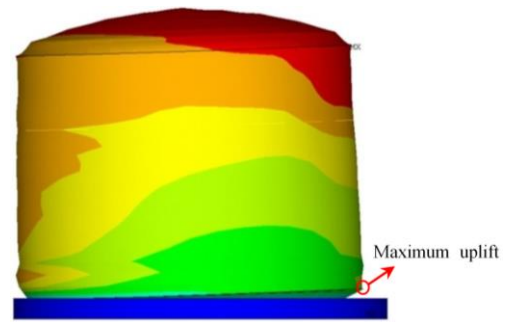


Fig. 9 The time-history of nonlinear response at the right endpoint of the tank bottom

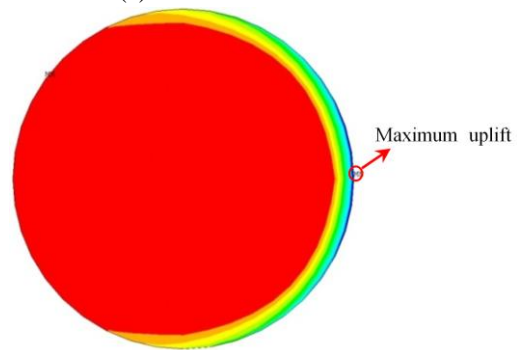
sharply increases in a short time after the peak earthquake appeared, and the slip has been increased and did not ultimately recover.

The maximum uplift at the tank bottom is given in Fig. 10. Fig. 10(a) presents that the obvious uplift deformation occurred at tank bottom due to the dynamic pressure effect of the liquid. The red area in Fig. 10(b) means no uplift, and other colors areas represent different degrees of uplift. The uplift deformation mainly occupies a narrow crescent-shaped area in the outer edge of the bottom. No overturning occurred due to uplift, and the area is very small. The slip at the tank bottom at the Class-IV site at the end of the seismic wave input is presented in Fig. 11. It is seen that, on the right bottom of the tank, the red dotted line is the location of the tank at the beginning of earthquake. At the end of earthquake, the obvious unrecoverable sliding displacement occurred at the tank bottom along the lateral direction, as shown in the green dotted line.

Table 7 lists the maximum uplift and slippage



(a) Deformation of the tank



(b) The uplift area at the tank bottom

Fig. 10 The nonlinear deformation of tank at the Class-I site ( $t = 6.84$  s)

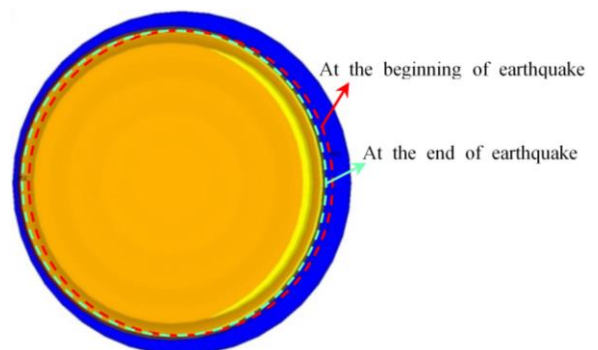


Fig. 11 The tank bottom slippage at the Class-IV site

Table 7 Results of maximum uplift and slippage at the tank bottom

Site Type	Maximum Uplift (mm)	Occurred Time (s)	Time of Peak Seismic Wave (s)	Slippage at Left Bottom (mm)	Slippage at Right Bottom (mm)
Class-I	6.7	6.84	6.68	11.4	7.9
Class-II	4.0	4.42	4.36	6.1	4.0
Class-III	2.5	8.65	8.60	3.7	0.6
Class-IV	5.8	7.42	7.33	18.4	23.5

calculations at the bottom of the tank. Due to the lag in the hydraulic pressure acting on the tank, the moments of maximum uplift that occurred are a bit later than the time of the peak seismic waves, which is the lag phenomenon at the bottom uplift of the tank and the input seismic wave. There are more high frequency components in the seismic wave on the Class-I site, and the maximum uplift occurs at the right end of the tank bottom. The uplift height of 6.7 mm occurred at 6.84 s, which occurred at the same time as the time when the largest elephant-foot deformities on the left side wall of the tank in the previous analysis occurred. At the Class-III site, the minimum uplift height is 2.5 mm, differing from the 62.69% from the Class-I site. Indeed, the tank uplift is affected not only by the high-frequency seismic waves but also by the liquid sloshing. The liquid sloshing is the greater, so the overturning moment will produce uplift more easily.

At the Class-IV site, the slippage at the left tank bottom increases from 1.3 mm (at 7.06 s) to 23 mm (at 13.05 s), while the right side increases from 0.6 mm (at 5.04 s) to 17.8 mm (at 12.85 s), which takes approximately seven seconds. The growth rate of slippage is not as great as that at the Class-I site. The reason is that at the Class-IV site, the duration time of the larger seismic wave energy is longer, so that more time is needed for the maximum slippage amount of the bottom. Moreover, sliding deformation is unrecoverable and eventually leads to the maximum horizontal slippage of the tank bottom.

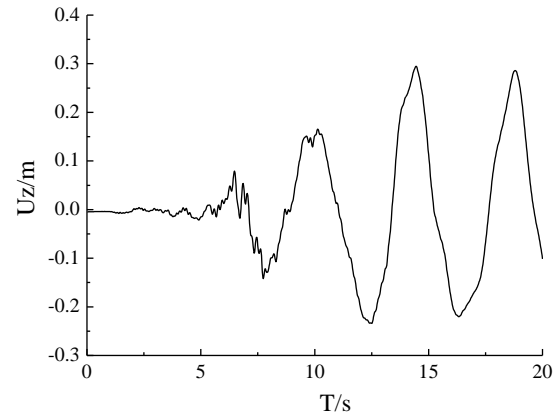
#### 5.4 Vertical sloshing of liquid inside the tank

The results show that the sloshing wave time-history curves along the liquid surface are symmetrical at both the left and the right end. Alternately, on both sides of the liquid sloshing, the amplitude of the free surface in contact with the tank wall is most significant. Here are the right end and the left end of the free liquid surface for analysis.

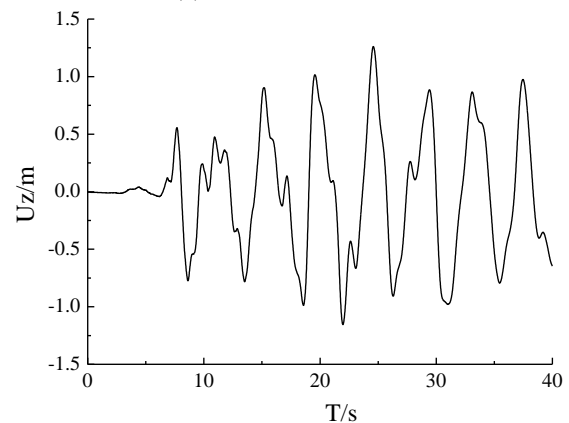
##### 5.4.1 Sloshing wave on the free liquid surface

The vertical shaking time-history curve results on the free surface of the tank liquid at the Class-I and Class-III sites are presented in Fig. 12.

Fig. 12 shows that there are obvious sloshing deformations on the free surface because the end points are in contact with the tank wall, and the absorptive capacity



(a) At the Class-I site



(b) At the Class-III site

Fig. 12 Time-history of the vertical sloshing on the free liquid surface

of the energy generated by liquid sloshing of the wall is relatively weak. The liquid produces a great impact force on the tank wall. Within 20 seconds of the duration of seismic waves, a large-amplitude substantial vertical sloshing was completed with three and a half periods under input of a seismic wave at the Class-I site. Within 40 seconds of the duration of the seismic waves, seven and a half periods were completed for the Class-III site.

Under the action of the seismic waves, the liquid does not produce a sloshing response at the beginning and maintains the tiny state for a long time. When the time increases, the seismic waves are growing, and the vertical sloshing is also increasing. Because there are large differences between the modulus of the liquid and the tank, the sloshing wave height reactions lag behind the earthquake. Greater vertical sloshing excitation needs a longer time. However, the liquid sloshing has begun, and the liquid sloshing will not decrease and stop correspondingly with the decrease in the seismic excitation, but the sloshing response may continue to increase. The reason is that, although seismic wave excitation is reduced, the input of energy continues to increase, and the sloshing amplitude continues to increase. Due to the lag effect of the liquid, when the earthquake stops, the shaking does not stop immediately, but free vibration occurs continually. When the earthquake stops, the fluctuation will continue for some time due to the inertia effect, which is most obvious at the

Class-IV site.

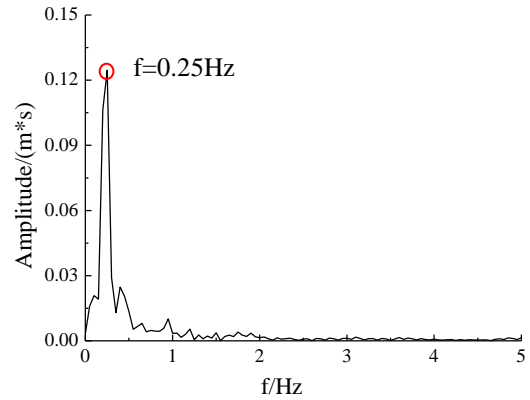
#### 5.4.2 Vertical sloshing displacement

The maximum vertical sloshing results are listed in Table 8. To analyze the effect of the spectral characteristics of the seismic waves on the sloshing of the free surface, Table 8 also gives the predominant periods of sloshing time-history and input seismic waves.

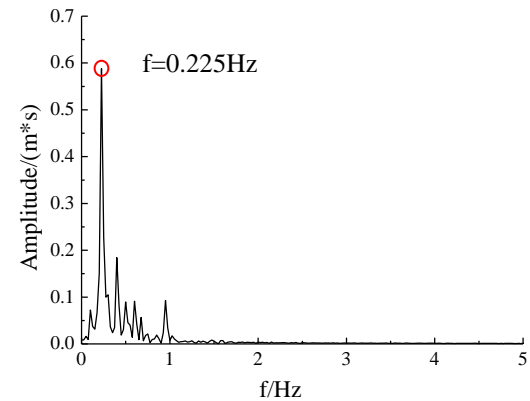
According to Table 8, the maximum vertical sloshing displacement reaches 1.262 m at the Class-III site. The minimum shaking value occurs on the Class-II site, 0.2 m, and there is a difference of 84.15% between the maximum and minimum shaking values. According to the code (GB50341-2014 2014), for the fixed roof tanks, the distance from the highest design level to the top tank wall should be greater than the sloshing wave height of the liquid surface. In this study, the distance is 1.8 m, the maximum sloshing in all four cases does not exceed the maximum height. If necessary, some measures can be taken to reduce liquid sloshing to avoid substantial liquid sloshing and leaking of liquid at the Class-III site.

The peak vertical sloshing of the liquid free surface is relative to the basic sloshing period of the liquid, and the influence is very clear with the type of site earthquake wave input recorded. To analyze the spectral characteristics of the sloshing response under Class-I and Class-III site conditions, the Fourier spectrum of vertical sloshing is shown in Fig. 13.

Fig. 13 and Table 8 present that the vertical sloshing response of the free surface shows a very obvious long periodicity. According to the spectral analysis, all the basic sloshing periods range from 4 s to 5 s, very close to the basic sloshing period of the liquid 4.39 s. This value also indicates that the basic sloshing mode of free surface makes the most significant contribution to the sloshing response. When the reasons for the differences at four sites are analyzed, the predominant period of the seismic wave is closest to the basic sloshing period at the Class-III site, and spectral values of the seismic wave are larger and concentrated near the predominant frequency area. Therefore, it brings the most energy, and the sloshing response at the Class-III site is much greater than in the other cases. At the Class-II and Class-IV sites, the seismic predominant frequency is closer, but at the Class-IV site, the energy of the seismic waves near the dominant frequency is much greater than that at the Class-II site, so the sloshing value increases 2.23 times greater than that at the Class-II site. The predominant frequency for Class-I and



(a) At the Class-I site



(b) At the Class-III site

Fig. 13 Fourier spectrum of vertical sloshing of the free liquid surface

Class-II sites differs significantly, but their energy is all concentrated at the predominant frequency area and away from the basic sloshing frequency. In this way, it is difficult to stimulate sloshing modes, thus, the sloshing amplitudes of both site conditions are all a little different and are much smaller compared with the results of the other sites.

Therefore, the seismic design of the large tank should avoid closeness between the predominant period of the seismic waves and the liquid sloshing period. Further, the seismic design of the large tank should pay attention to the significant sloshing height caused by the ground motion at the soft sites. If necessary, the influence of long period seismic waves should be checked, and necessary measures to reduce the sloshing of liquid should be taken to avoid the leakage of liquid, which may lead to serious consequences.

Table 8 Calculation results of maximum vertical sloshing amplitude of free liquid surface

Site Class	Peak Sloshing Displacement (m)	Sloshing Feature		Seismic Wave Feature	
		Corresponding Time (s)	Sloshing Fundamental Period (s)	Corresponding Time (s)	Predominant Period (s)
Class-I	0.295	14.46	4.00	6.68	0.20
Class-II	0.238	4.41	5.00	4.36	0.38
Class-III	1.262	24.58	4.44	8.60	1.67
Class-IV	0.768	17.15	4.00	7.33	0.36

Table 9 Results of base shear and overturning moment

Site Type	Base shear ( $10^6$ N)	Time (s)	Overturning Moment ( $10^7$ N·m)	Time (s)
Class-I	4.97	6.96	2.606	6.94
Class-II	4.66	4.53	2.157	4.57
Class-III	4.51	8.61	1.989	10.55
Class-IV	4.90	9.95	2.516	9.94

### 5.5 Base shear and overturning moment of the tank

The base shear and overturning moment of the tank are calculated under four types of field conditions. The results of peak values are listed in Table 9.

The predominant period of record seismic waves at the Class-I site and the basic period of the tank-liquid coupling vibration is closer, so the base shear and overturning moment is the maximum,  $4.97 \times 10^6$  N and  $2.606 \times 10^7$  N·m, respectively. However, the predominant period of seismic wave at Class-III is farthest from the basic period of the tank liquid coupling vibration, so the minimum results are produced. Under the input of four seismic waves, the difference between maximum and minimum values of the overturning moment and base shear response are 23.68% and 9.26%, respectively, which shows that the impact of the type of site on the base shear response is relatively small.

### 5.6 Discussion

Through the previous deformation and stress analysis of the tank wall, the deformation close to the elephant-foot location does not reach the yield limit of the material. However, the axial compressive stress exceeds the allowable compressive stress values specificity in the code. Therefore, the deformation of the elephant-foot with a horizontal earthquake belongs to the partial buckling damage induced by the axial compressive stress exceeding the critical buckling stress, not the strength damage of the material. Therefore, when making a seismic design for a large volume tank, the focus should be on improving the allowable compressive stress of the tank wall and increasing the wall thickness of the tank to prevent local buckling damage resulting from failure of the tank, causing serious consequences.

Clearly, the slip of the tank bottom has a direct relationship to the spectrum and the waveform of the seismic wave and should bring attention to the impact of the site type, if necessary, to take certain restrictive measures at the bottom of the tank to avoid a large slippage, which may cause serious damage to tank bottom plate.

## 6. Conclusions

In this study, horizontal seismic response analysis for an unanchored tank was conducted under four seismic waves recorded on different class of soil sites. The numerical model of tank with full liquid was established using

ANSYS software. Modal periods, elephant-foot buckling, sloshing, uplift and slip, base shear and overturning moment were studied. Concluding remarks obtained from this research can be summarized as follows.

- The obvious elephant-foot deformation occurred at height 1.2 m, close to the tank bottom. At the four types of sites, all the maximum stress on the tank wall did not exceed the yield stress of the material. However, the axial compressive stress near the elephant-foot area at the Class-I and Class-IV site exceeds the allowable compressive stress values specified in the code, resulting in local buckling failure. Tank wall thickness can be increased appropriately, and the allowable compressive stress of the tank wall can be increased to prevent local buckling failure.
- Nonlinear uplift and slip deformation happened at the tank bottom, and the maximum uplift value achieves 6.7 mm at the Class-I site. The slippage at the end of earthquake reached 23.5 mm at the Class-IV site, which indicates that the tank container exhibits dangerous destruction and may cause leakage of liquid. When the seismic design for the tank is carried out, the design should take some appropriate limiting measures to reduce uplift and slip of the tank bottom
- The maximum vertical sloshing displacement on the free surface reaches 1.26 m at the Class-III site, which obviously shows the characteristics of a long period and is dangerous. It should avoid that the predominant period of the liquid sloshing close to the predominant period of the seismic waves. If necessary, some measures can be taken to reduce liquid sloshing and to prevent spilling of liquid due to the significant sloshing.

## Acknowledgments

The research described in this paper was financially supported by the National Natural Science Foundation of China (Grant No. 51408609) and Shandong Province Higher Educational Science and Technology Program (Grant No. J14LG51).

## References

- ANSYS Inc. (2012), <http://www.ansys.com>.
- ANSYS software. (2007), *Engineering simulation software, version 14*. Pennsylvania, United States: Canonsburg.
- Bayraktar, A., Sevim, B., Altunışık, A.C. and Türker, T. (2010), "Effect of the model updating on the earthquake behavior of steel storage tanks", *J. Constr. Steel. Res.*, **66**(3), 426-469.
- Cooper, T.W. and Wachholz, T.P. (1999), "Optimizing post-earthquake lifeline system reliability", *Proceeding of the 5th US Conference on Lifeline Earthquake Engineering*, Seattle, USA, August.
- Curadelli, O. (2013), "Equivalent linear stochastic seismic analysis of cylindrical base-isolated liquid storage tanks", *J. Constr. Steel. Res.*, **83**(2), 166-176.
- GB 50341-2014 (2014), Code for Design of Vertical Cylindrical Welded Steel Oil Tanks, Ministry of Housing and Urban-Rural Development of the People's Republic of China, Beijing, China.
- Goudarzi, M.A. and Sabbagh-Yazdi, S.R. (2009), "Numerical

- investigation on accuracy of mass spring models for cylindrical tanks under seismic excitation”, *Int. J. Civ. Eng.*, **7**(3), 190-202.
- Haroun, M.A. (1983), “Vibration studies and test of liquid storage tanks”, *Earthq. Eng. Struct. D.*, ASCE, **11**(2), 179-206.
- Hesamaldin, M., Masoud, M. and Touraj, T. (2014), “Probabilistic analysis of seismically isolated elevated liquid storage tank using multi-phase friction bearing”, *Earthq. Struct.*, **6**(1), 111-125.
- Hosseinzadeh, N., Kazem, H., Ghahremannejad, M., Ahmadi, E. and Kazem, N. (2013), “Comparison of API650-2008 provisions with FEM analyses for seismic assessment of existing steel oil storage tanks”, *J. Loss. Prevent. Proc.*, **26**(4), 666-675.
- Li, J.Y., You, X.C., Cui, H.C. and Ju, J.S. (2015), “Analysis of large concrete storage tank under seismic response”, *J. Mech. Sci. Technol.*, **29**(1), 85-91.
- Liu, M. and Gorman, D.G. (1995), “Formulation of Rayleigh damping and its extensions,” *Comput. Struct.*, **57**(2), 277-285.
- Livaoglu, R. and Dogangun, A. (2007), “Effect of foundation embedment on seismic behavior of elevated tanks considering fluid-structure-soil interaction”, *Soil. Dyn. Earthq. Eng.*, **27**(9), 855-863.
- Ma, Q.L., Lu, X.Z. and Ye, L.P. (2008), “Influence of the inter-story post-yield stiffness to the variance of seismic response”, *Eng. Mech.*, **25**(7), 133-141.
- Newmark, N.M. (1959), “A method of computation for structural dynamics”, *J. Eng. Mech.*, ASCE, **85**(1), 67-94.
- Newmark, N.M. and Rosenblueth, E. (1971), *Fundamentals of earthquake engineering*, Prentice-Hall, Englewood Cliffs, NJ, USA.
- Ormeño, M., Larkin, T. and Chouw, N. (2015), “Evaluation of seismic ground motion scaling procedures for linear time-history analysis of liquid storage tanks”, *Eng. Struct.*, ASCE, **102**, 266-277.
- Park, J.H., Bae, D. and Chang, K.O. (2016), “Experimental study on the dynamic behavior of a cylindrical liquid storage tank subjected to seismic excitation”, *Int. J. Steel. Struct.*, **16**(3), 935-945.
- Seleemah, A.A. and Mohamed, E.S. (2011), “Seismic analysis and modeling of isolated elevated liquid storage tanks”, *Earthq. Struct.*, **2**(4), 397-412.
- Udwadia, F.E. and Tabaie, S. (1981), “Pulse control of single degree-of-freedom system”, *J. Eng. Mech. Div.*, ASCE, **107**(6), 997-1009.
- Velersos, A.S. and Yang, J.Y. (1977), “Earthquake response of liquid storage tanks”, *Proceedings of the First ASCE-EMD Specialty Conference on Mechanics in Engineering*, Raleigh, North Carolina, USA, May.